



Simulation of sloshing motions in fixed and vertically excited containers using a 2-D inviscid σ -transformed finite difference solver

J.B. Frandsen^{a,*}, A.G.L. Borthwick^b

^a *Department of Civil and Environmental Engineering, Louisiana State University, Baton Rouge, LA 70803, USA*

^b *Department of Engineering Science, University of Oxford, Parks Road, Oxford OX1 3PJ, UK*

Received 3 January 2003; accepted 18 July 2003

Abstract

Nonlinear effects of standing wave motions in fixed and vertically excited tanks are numerically investigated. The present fully nonlinear model simulates two-dimensional waves in stable and unstable regions of the free-surface flow. Numerical solutions of the governing nonlinear potential flow equations are obtained using a finite-difference time-stepping scheme on adaptively mapped grids. A σ -transformation in the vertical direction that stretches directly between the free surface and bed boundary is applied to map the moving free-surface physical domain onto a fixed computational domain. A horizontal linear mapping is also applied, so that the resulting computational domain is rectangular, and consists of unit square cells.

Predictions of small-amplitude free-surface motions in fixed and vertically excited tanks compare well with second order small perturbation theory. For stable steep waves in the vertically excited tank, the free surface exhibits nonlinear behaviour. Parametric resonance is evident in the instability zones, as the amplitudes grow infinitely large, even for small forcing amplitudes. For steep initial amplitudes the predictions differ considerably from the small perturbation theory solution, demonstrating the importance of nonlinear effects.

The present numerical model provides a simple way of simulating steep nonbreaking waves. It is computationally quick and accurate. The σ -transformation removes the need for free-surface smoothing for the cases considered herein.

© 2003 Published by Elsevier Ltd.

1. Introduction

Free-surface motions of liquid under gravity in tanks are of practical importance, particularly in marine applications. Examples include liquid sloshing in ship tanks which may cause the ship to undergo large rolling motions, and free-surface-induced forces on the walls of storage containers on offshore platforms. In civil engineering, tuned liquid dampers are used to suppress wind-induced vibrations of tall buildings (Kareem et al., 1999), and to limit resonant damage of liquid storage tanks in seismic zones. Further applications in the aerospace industry are described by Abramson (1966). In order to predict the maximum forces due to the liquid responses to excitation, it is essential to be able to model steep waves properly during sloshing cycles, particularly as nonlinear effects become significant as the wave amplitude increases.

Considerable previous theoretical and experimental research studies have been carried out into liquid sloshing in fixed and moving tanks. Faltinsen (1978), Faltinsen and Timokha (2002) and Frandsen (2003) present approximate

*Corresponding author.

E-mail address: frandsen@lsu.edu, jannette.frandsen@eng.ox.ac.uk (J.B. Frandsen).

theoretical forms for inviscid sloshing motion in fixed and moving tanks. Recently, Wu et al. (2001) derived an analytical solution for viscous sloshing in rectangular tanks. The foregoing low-order analytical solutions are very useful for gaining understanding of small amplitude motions in tanks, and for validating numerical models. However, physical experiments and numerical modelling are necessary for steep free-surface motions because neither linear nor second-order theory is applicable when high-order effects are significant. Using a laboratory vertically oscillating tank facility, Bredmose et al. (2003) have measured highly nonlinear “flat-topped” free-surface profiles caused by harmonically forced vertical accelerations (representing heave excitations). With a view to ship applications where heave motions are less significant, Faltinsen and Timokha (2002) describe sloshing motion experiments in tanks forced to rotate and move in the horizontal direction.

To date most numerical models treat the moving free-surface boundary in one of two ways: either by using Lagrangian tracking of free-surface nodes with regridding, or by mappings. The former has the disadvantage that the surface velocities are difficult to predict correctly, and so free-surface smoothing is required. Although mappings inherently overcome this problem, they are less flexible to apply to irregular geometries or to cases where submerged bodies are present in the flow domain. Many numerical studies have been undertaken into sloshing in fixed and moving tanks. For example, Telste (1985) modelled the time-dependent behaviour of the free surface of an inviscid liquid in a 2-D tank by means of a finite difference model. Chen et al. (1996) used a finite difference model to examine large sloshing motions in 2-D tanks excited by the horizontal component of four seismic events. For nonoverturning waves, Chen et al.’s model demonstrated that nonlinear effects during certain earthquakes could be sufficiently large to damage tanks. Chern et al. (1999) and Turnbull et al. (2003) simulated 2-D free and forced inviscid sloshing using linearly stretched σ -transformed mappings in pseudospectral and finite element schemes. Ferrant and Le Touze (2001) applied an inviscid pseudo-spectral model to predict 3-D sloshing motions. Wu et al. (1998) also studied the behaviour of nonbreaking standing waves in 3-D tanks. Using inviscid fluid finite elements, Wu et al. focused on near resonance cases in tanks excited by both sway and surge motions. Furthermore, Ushijima (1998) used an arbitrary Lagrangian–Eulerian method on boundary-fitted grids to analyse viscous sloshing and swirling effects in a 3D cylindrical tank.

The present paper describes a 2-D fully nonlinear numerical model of liquid sloshing motions in fixed and vertically excited rectangular tanks. It is assumed that the liquid is inviscid, incompressible and irrotational, that the free surface does not become vertical or overturn, and that surface tension can be neglected. A modified σ -transformation that stretches the grid from the bed to the free surface is combined with a horizontal linear mapping, so that the resulting fixed computational domain is rectangular with cell increments of unit dimensions (thus simplifying the discretized equations). The governing equations and boundary conditions expressed in terms of the velocity potential are mapped accordingly, and discretized using second-order finite differences. The σ -transformation has two major advantages. Remeshing due to the moving free surface is not required; and the free surface velocity components are not explicitly needed as part of the computation process. Extrapolations are unnecessary, and so free-surface smoothing by means of a spatial filter is not required. The motivation behind this is that equivalent solutions on 2-D grid with σ -transformation are known to be extremely stable (Chern et al., 1999; Turnbull et al., 2003), unlike other schemes which have to use free surface smoothing.

The numerical model is validated by simulating standing waves of different fundamental wavelengths in fixed rigid rectangular tank. Increasing wave steepness is considered in order to demonstrate the effects of high-order nonlinearities on the wave forms, unobtainable with first- and second-order analytical solutions. In such cases, the fully nonlinear model is required. Then, numerical investigations are undertaken into sloshing effects in vertically excited tanks. Standing waves generated in vertically oscillating tanks through sub-harmonic resonance were first studied experimentally by Faraday (1831). Benjamin and Ursell (1954) investigated Faraday waves theoretically. Their analyses were based on an inviscid flow model with surface tension, and they found that small amplitude wave motion is governed by the Mathieu equation. Benjamin and Ursell concluded that the linearized solutions are always unstable for an external forcing frequency equal to twice the sloshing frequency. A comprehensive review has been given by Miles and Henderson (1990). The present model investigates the consequences of eliminating the nonlinear terms.

The results presented herein have been computed on a SUN Ultra 60 workstation with 450MHz CPU (SPECfp95: 32.7). In no case did the CPU time required exceed 2 h or the RAM required exceed 12 MB.

2. Governing equations

In the following idealized fluid model, we assume the fluid to be incompressible, irrotational and inviscid, and therefore governed by Laplace’s equation

$$\frac{\partial^2 \phi}{\partial x^2} + \frac{\partial^2 \phi}{\partial z^2} = 0, \quad (1)$$

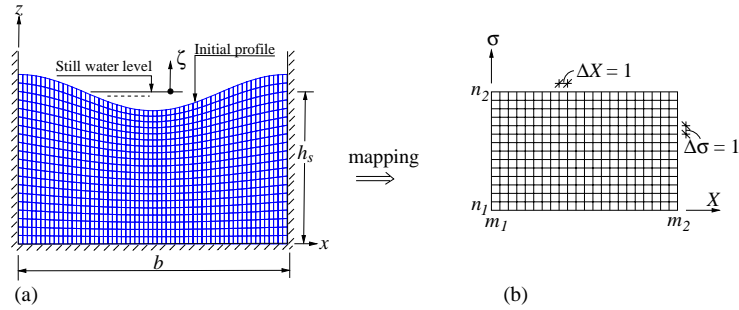


Fig. 1. The physical domain (a) mapped onto the computational domain (b).

where ϕ is the velocity potential function and x and z are horizontal and vertical distances in a Cartesian coordinate system, as shown in Fig. 1.

We assume a flat bed and that waves are generated in a tank with solid walls. The fluid velocity components normal to fixed boundaries are equal to zero by definition. Hence, we have

$$\frac{\partial \phi}{\partial x} = 0, \quad x = 0, b, \tag{2}$$

$$\frac{\partial \phi}{\partial z} = 0, \quad z = 0. \tag{3}$$

The dynamic free-surface boundary condition is

$$\frac{\partial \phi}{\partial t} = -g\zeta(x, z, t) - \frac{1}{2} \left[\left(\frac{\partial \phi}{\partial x} \right)^2 + \left(\frac{\partial \phi}{\partial z} \right)^2 \right], \tag{4}$$

where g is the acceleration due to gravity and ζ is the free-surface elevation measured vertically above still water level.

The kinematic free-surface boundary condition is

$$\frac{\partial \zeta}{\partial t} = \frac{\partial \phi}{\partial z} - \frac{\partial \phi}{\partial x} \frac{\partial \zeta}{\partial x}. \tag{5}$$

3. Modified σ -transformed formulation

The σ -transformation was first used by Phillips (1957) for weather prediction. Later it was used by Mellor and Blumberg (1985) for ocean modelling, and it has since been widely applied to shallow water flows (see e.g. Kocycit et al., 2002) and to simulate waves in relatively deep water (see e.g. Turnbull et al., 2003). In the present paper, a modified σ -transformation is used to map the liquid domain onto a rectangle, such that the moving free surface in the physical plane becomes a fixed horizontal line in the computational mapped domain. Fig. 1 illustrates the effect of the mapping, which has been designed so that each computational cell in the transformed domain is of unit size. The mapping implicitly deals with the free surface motion, and avoids the need to calculate the free surface velocity components explicitly. Extrapolations are unnecessary, and so free-surface smoothing by means of a spatial filter is not required for the results presented here. It should be noted that the mapping is linear between the bed and free surface, which is unique by definition, and so the model is limited to nonvertical free-surface profiles, thus excluding overturning waves.

With reference to Fig. 1, the mappings from the physical (x, z, t) domain to the transformed (X, σ, T) domain are given by

$$\begin{aligned} x &\leftrightarrow X, & X &= m_1 + \frac{(m_2 - m_1)}{b} x, \\ z &\leftrightarrow \sigma, & \sigma &= n_1 + \frac{(n_2 - n_1)(z + h_s)}{h}, \\ t &\leftrightarrow T, & T &= t, \end{aligned} \tag{6}$$

where m_1, m_2, n_1 and n_2 refer to nodal indices of the corner points of the grid in the mapped domain.

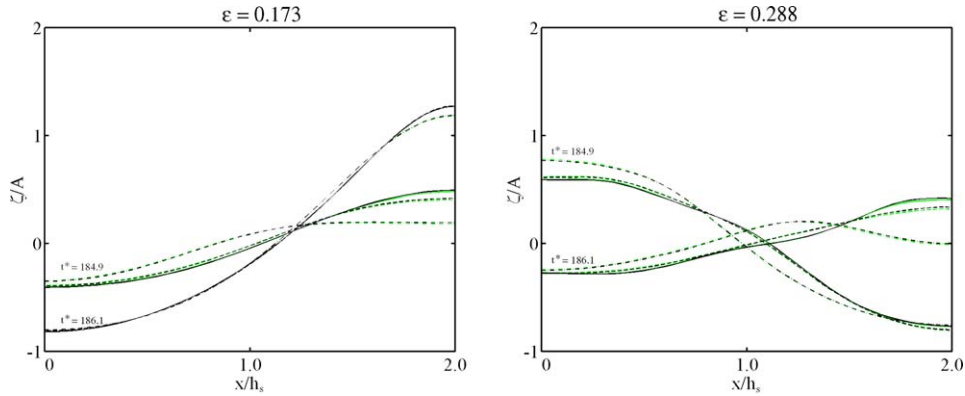


Fig. 2. Free-surface profiles ($n = 1$) for $\Delta t^* = 0.011$ (dark curves) and $\Delta t^* = 0.006$ (light curves). Grid: $-\cdot-$, 40×20 ; $-$, 40×40 ; $-$, 40×80 .

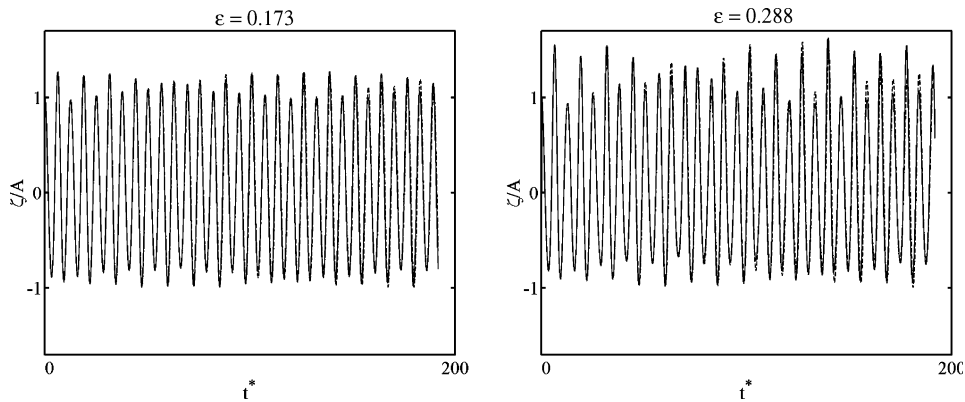


Fig. 3. Free-surface elevation at the left wall ($n = 1$) for $\Delta t^* = 0.011$. Grid: $-$, 40×20 ; $-$, 40×80 .

The derivatives of the potential function $\phi(x, z, t)$ are transformed with respect to x, z and t into derivatives of $\Phi(X, \sigma, T)$. The first derivatives of the velocity potential, ϕ , are obtained as

$$\begin{aligned} \frac{\partial \phi}{\partial x} &= \frac{(m_2 - m_1)}{b} \left(\frac{\partial \Phi}{\partial X} + \frac{\alpha}{h} \frac{\partial \Phi}{\partial \sigma} \right), \\ \frac{\partial \phi}{\partial z} &= \frac{(n_2 - n_1)}{h} \frac{\partial \Phi}{\partial \sigma}, \\ \frac{\partial \phi}{\partial t} &= \frac{\partial \Phi}{\partial T} + \frac{\gamma}{h} \frac{\partial \Phi}{\partial \sigma}, \end{aligned} \tag{7}$$

where $\alpha = -(\sigma - n_1)\partial\zeta/\partial X$ and $\gamma = -(\sigma - n_1)\partial\zeta/\partial T$.

Similarly, Laplace's equation (1) can be rewritten as

$$\frac{\partial^2 \Phi}{\partial X^2} + \frac{1}{h} \left[\frac{\partial \alpha}{\partial X} - \frac{2\alpha}{h} \frac{\partial h}{\partial X} \right] \frac{\partial \Phi}{\partial \sigma} + 2 \frac{\alpha}{h} \frac{\partial^2 \Phi}{\partial \sigma \partial X} + \left[\frac{\alpha^2}{h^2} + \frac{b^2(n_2 - n_1)^2}{h^2(m_2 - m_1)^2} \right] \frac{\partial^2 \Phi}{\partial \sigma^2} = 0. \tag{8}$$

In the following, we rewrite the boundary conditions (2)–(5) using the σ -transformation.

The fixed vertical wall boundary condition (2) on $X = m_1$ and m_2 is

$$\frac{\partial \Phi}{\partial X} = -\frac{\alpha}{h} \frac{\partial \Phi}{\partial \sigma}, \tag{9}$$

where $h = \zeta + h_s$; and the still water depth is h_s .

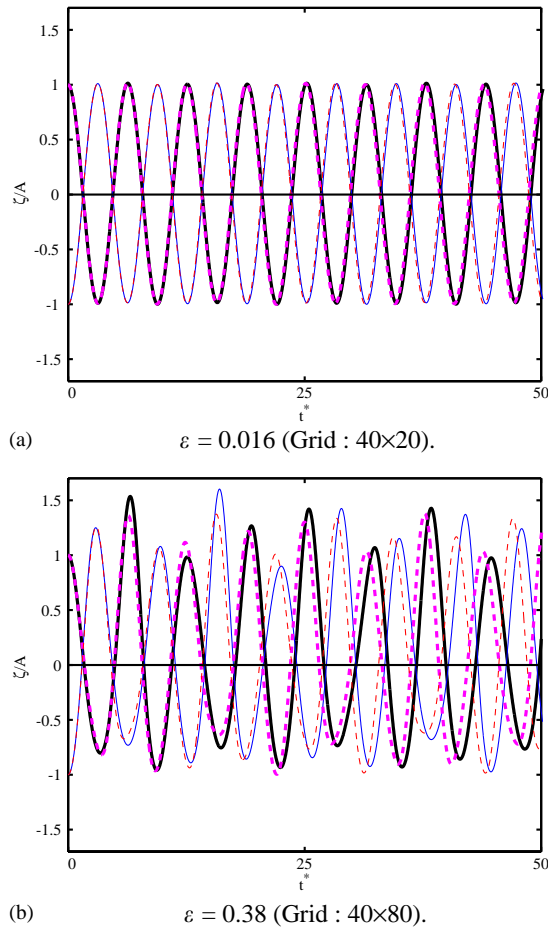


Fig. 4. Free-surface elevation at the left wall and tank centre ($n = 2$) for $\omega_2 = 5.54$ rad/s. (a) $\varepsilon = 0.016$ (Grid: 40×20). (b) $\varepsilon = 0.38$ (Grid: 40×80). —, Numerical prediction at left wall; —, numerical prediction at tank centre; - -, second-order solution at left wall; - -, second-order solution at tank centre.

The flat bed boundary condition (3) on $\sigma = n_1$ becomes

$$\frac{(n_2 - n_1)}{h} \frac{\partial \Phi}{\partial \sigma} = 0 \rightarrow \frac{\partial \Phi}{\partial \sigma} = 0. \tag{10}$$

The dynamic free-surface boundary condition (4) on $\sigma = n_2$ becomes

$$\frac{\partial \Phi}{\partial T} = \frac{(n_2 - n_1)}{h} \frac{\partial \zeta}{\partial T} \frac{\partial \Phi}{\partial \sigma} - g\zeta - \frac{1}{2} \left[\frac{(m_2 - m_1)^2}{b^2} \left(\frac{\partial \Phi}{\partial X} - \frac{(n_2 - n_1)}{h} \frac{\partial \zeta}{\partial X} \frac{\partial \Phi}{\partial \sigma} \right)^2 + \frac{(n_2 - n_1)^2}{h^2} \left(\frac{\partial \Phi}{\partial \sigma} \right)^2 \right] \tag{11}$$

and the kinematic free-surface boundary condition (5) on $\sigma = n_2$ becomes

$$\frac{\partial \zeta}{\partial T} = \frac{(n_2 - n_1)}{h} \frac{\partial \Phi}{\partial \sigma} \left[1 + \frac{(m_2 - m_1)^2}{b^2} \left(\frac{\partial \zeta}{\partial X} \right)^2 \right] - \frac{(m_2 - m_1)^2}{b^2} \frac{\partial \zeta}{\partial X} \frac{\partial \Phi}{\partial X}. \tag{12}$$

Eqs. (8)–(12) are spatially discretized using second-order finite differences and solved in the transformed domain iteratively using successive over-relaxation. Furthermore, the unsteady free-surface boundary equations are temporally discretized using the second-order Adams–Bashforth scheme.

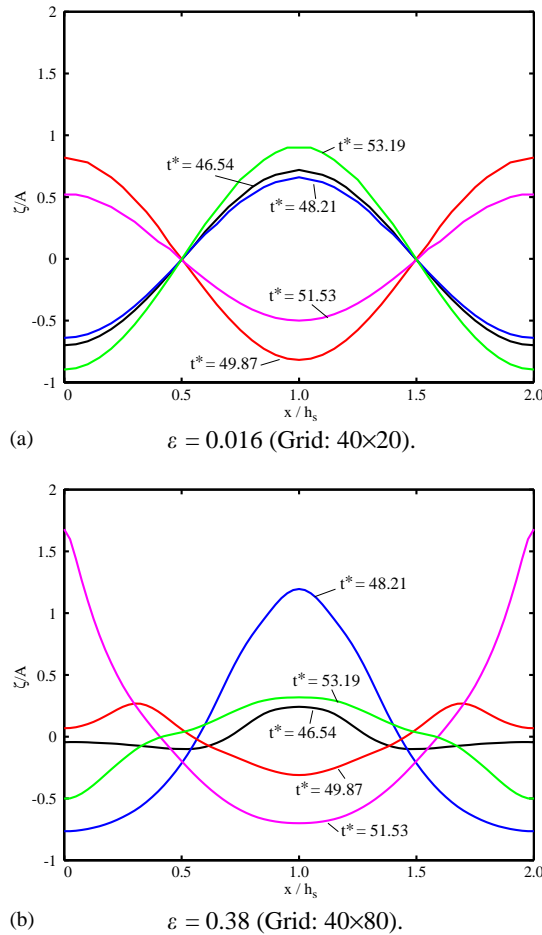


Fig. 5. Free-surface profiles for $n = 2$. (a) $\varepsilon = 0.016$ (Grid: 40×20). (b) $\varepsilon = 0.38$ (Grid: 40×80).

4. Sloshing motions in 2-D fixed tanks

Inviscid free sloshing in a fixed rectangular tank is chosen as a benchmark validation test.

Numerical predictions of the free surface motions are compared with analytical results from second-order potential theory. Second-order solutions of liquid motions in a 2-D rectangular tank can be obtained by representing the velocity potential as an expansion based on the eigensolutions of free sloshing motions:

$$\phi = \sum_n \frac{\cosh(k_n(z + h_s))}{\cosh(k_n h_s)} \cos(k_n x) T_n(t), \tag{13}$$

where $k_n = n\pi/b$ is the wavenumber for $n = 0, 1, 2, \dots$. The ordinary differential equations for the functions T_n describe the time evolution of the individual components. These functions are obtained after substituting Eq. (13) into homogeneous first-order or nonhomogeneous second-order free-surface conditions. Solutions of the form (13) satisfy both the Laplace equation and the no-flow boundary condition on the tank walls. The second-order free-surface elevation for the n th sloshing mode along the length of the tank may then be expressed:

$$\begin{aligned} \zeta(x, t) = A & \left(\cos(\omega_n t) \cos(k_n x) + \frac{A\omega_n^2}{g} \left(\frac{1}{8} \frac{\omega_n^4 + g^2 k_n^2}{\omega_n^4} + \left(\frac{1}{8} \frac{3\omega_n^4 - g^2 k_n^2}{\omega_n^4} - \frac{3}{2} \frac{\omega_n^4 - g^2 k_n^2}{\omega_n^2(4\omega_n^2 - \omega_{2n}^2)} \right) \cos(2\omega_n t) \right. \right. \\ & \left. \left. + \frac{1}{2} \frac{\omega_n^2 \omega_{2n}^4 - \omega_n^4 - 3g^2 k_n^2}{\omega_n^2(4\omega_n^2 - \omega_{2n}^2)} \cos(\omega_{2n} t) \right) \cos(2k_n x) \right) + \dots, \end{aligned} \tag{14}$$

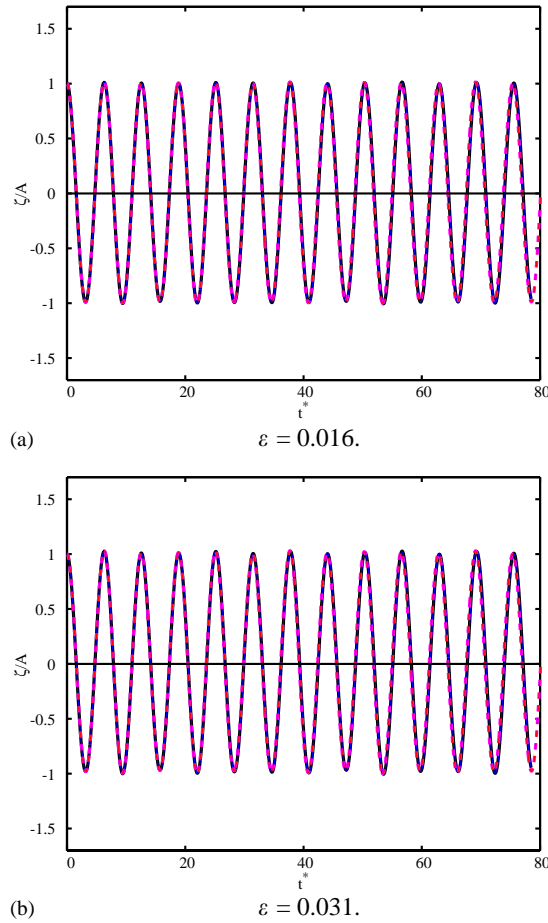


Fig. 6. Free-surface elevation at the left wall and tank centre for $\omega_4 = 7.9$ rad/s and a grid size of 40×80 . (a) $\varepsilon = 0.016$. (b) $\varepsilon = 0.031$. —, Numerical prediction at left wall; —, numerical prediction at tank centre; - -, second-order solution at left wall and tank centre.

where $\omega_n = \sqrt{gk_n \tanh(k_n h_s)}$ and $\omega_{2n} = \sqrt{g2k_n \tanh(2k_n h_s)}$. The initial conditions which satisfy the velocity potential and free-surface equations are chosen as

$$\zeta(x, n)|_{t=0} = A \cos(k_n x) \tag{15}$$

and

$$\phi(x, z)|_{t=0} = 0, \tag{16}$$

where A is the amplitude of the initial wave profile, and x is the horizontal distance from the left wall.

Nonlinear free-surface motions are investigated by varying the wave steepness, defined herein as $\varepsilon = A\omega_n^2/g$, where gravity is $g = 9.81$ m/s² until near breaking conditions are encountered. We note that ε is a measure of nonlinearity. The results presented are for a tank of aspect ratio $h_s/b = 0.5$, where b denotes the length of the tank. The linearly stretched grid in the physical domain in accordance with the σ -transformed equation (6) is shown in Fig. 1.

The time histories of the free sloshing motions are presented in nondimensional form using the sloshing frequency ω_n , so that the nondimensional time $t^* = \omega_n t$, and the nondimensional time step $\Delta t^* = \omega_n \Delta t$. The first numerical tests carried out are designed to check the sensitivity of the numerical scheme to the time step and the grid resolution.

Figs. 2 and 3 show wave profiles along the tank at two different times, and time histories of the free-surface elevation for the first sloshing mode ($n = 1$). Results for different grid resolutions are shown related to moderate and steep wave amplitudes ($\varepsilon = 0.173, 0.288$) for time steps of $\Delta t^* = 0.011$ and 0.006 . Increasing the grid points in the vertical direction was found to be more effective in improving accuracy than increasing the grid points in the horizontal direction. It was

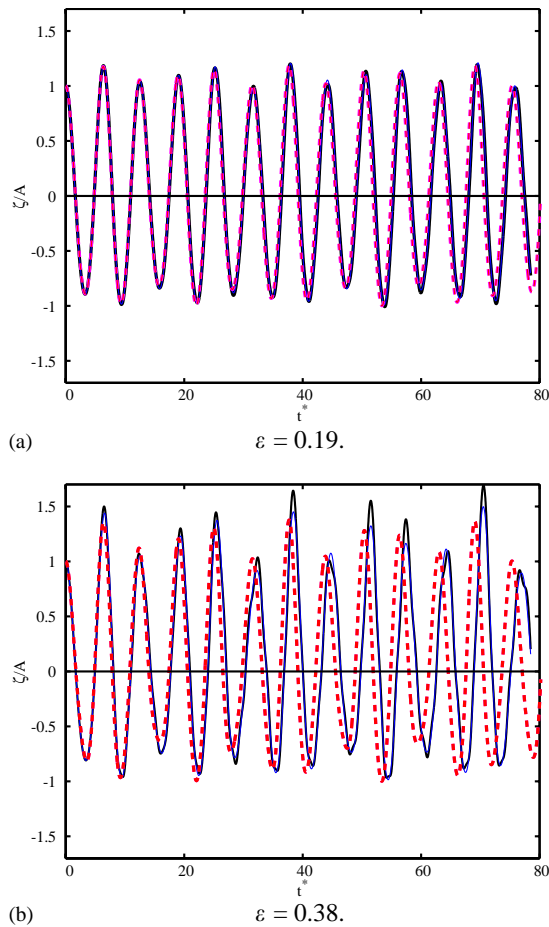


Fig. 7. Free-surface elevation at the left wall and tank centre for $\omega_4 = 7.9$ rad/s and a grid size of 40×80 . (a) $\varepsilon = 0.19$. (b) $\varepsilon = 0.38$. —, Numerical prediction at left wall; —, numerical prediction at tank centre; --, second-order solution at left wall and tank centre.

found that a grid size of 40×80 and a time step of 0.003 s provided sufficient accuracy to capture nonlinearities related to steep wave predictions ($\varepsilon > 0.2$).

Fig. 4 illustrates for $n = 2$ the time-dependent free-surface motion at the left wall and at the centre of the tank for (a) very small amplitude sloshing where $\varepsilon = 0.016$, and (b) large amplitude sloshing where $\varepsilon = 0.38$. Although a nondimensional time step of 0.017 was used in both cases, the grid size was increased in the vertical direction for the larger amplitude test case. A grid size of 40×40 and a nondimensional time step of 0.017 were sufficient to model accurately waves of small to moderate amplitude (approximately $\varepsilon < 0.09$), in comparison with the second-order analytical solution (14). For large amplitude sloshing it can be observed (Fig. 4b) that a phase-shift grows in time between the approximate analytical solution and the fully nonlinear numerical model prediction. Also the maximum amplitudes are higher and the troughs becomes less deep than those of the approximate solution. This has also been observed by Tadjbakhsh and Keller (1960), Vanden-Broeck and Schwartz (1981), Tsai and Jeng (1994) and Greaves et al. (1997). The corresponding numerical wave profiles across the tank at different times during a typical sloshing period are shown in Fig. 5. The small amplitude waves display linear standing waves whereas the steep wave case exhibits a dispersion effect that is most evident at the nodes at $x/h_s = 0.5$ and 1.5. Identical behaviour has been reported by other investigators, e.g., Chern et al. (1999).

Further studies were undertaken, halving the wavelength ($n = 4$). To maintain accuracy it was necessary to increase the mesh to 80 grid points in the vertical direction for the small amplitude wave cases. The non-dimensional time step was kept the same as for the single standing waves without violating the Courant condition. However, a further parameter test revealed that a factor of four decrease in the time step ($\Delta t^* = \omega_4 \Delta t = 0.0063$) did not have a significant effect for the single standing wave cases. Figs. 6 and 7 show the time histories of the free-surface elevation for increasing wave steepnesses ($\varepsilon \in [0.016, 0.38]$) at the centre of the tank and at the wall. For the double standing wave case, the

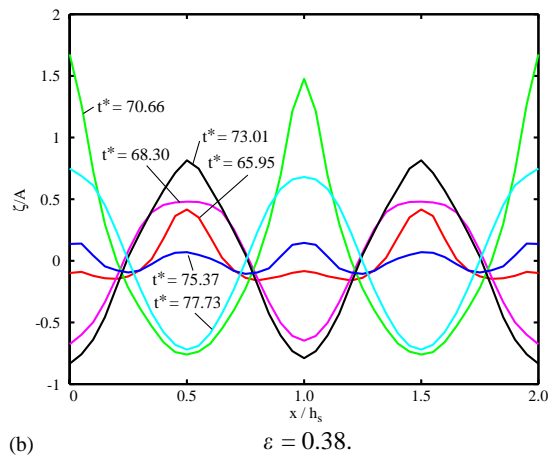
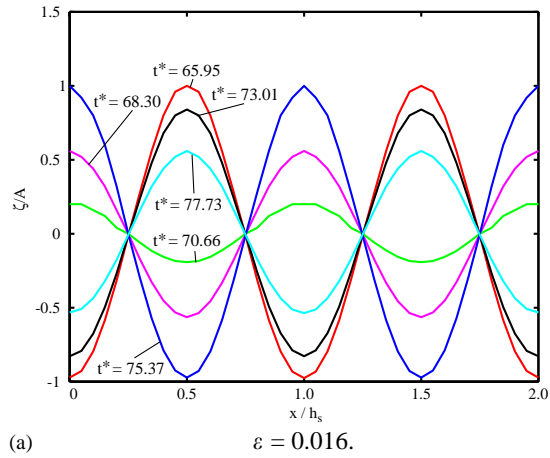


Fig. 8. Free-surface profiles for $n = 4$ and a grid size of 40×80 . (a) $\epsilon = 0.016$. (b) $\epsilon = 0.38$.

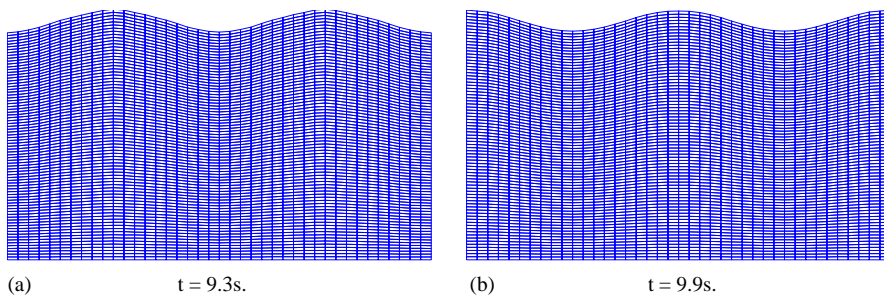


Fig. 9. Largest nonoverturning wave for $n = 4$ and $\epsilon = 0.38$. (a) $t = 9.3\text{ s}$. (b) $t = 9.9\text{ s}$.

phase-shift due to nonlinearity becomes evident for small wave steepnesses greater than 0.031 (Fig. 6b). Otherwise the same nonlinear patterns, but amplified, as for the single standing wave can be observed. In contrast to the single standing waves, the double standing wave free-surface elevations at the lateral walls and centre of the tank are in phase. However, the steepest wave case ($\epsilon = 0.38$) simulated by the fully nonlinear numerical model gives higher maximum peaks at the walls than the centre (Fig. 7b). Wave profiles for $n = 4$ are shown in Fig. 8 for a small wave steepness of $\epsilon = 0.016$ and for maximum steepness of $\epsilon = 0.38$ (just before the wave overturns/breaks). The large amplitude waves

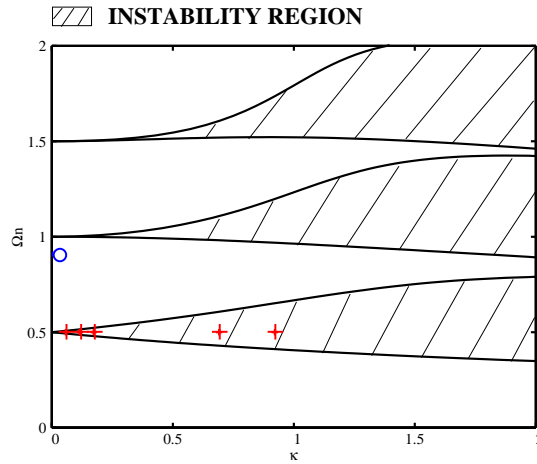


Fig. 10. Stability map for linear solutions of the vertically excited tank test cases: +, unstable solutions; o, stable solutions.

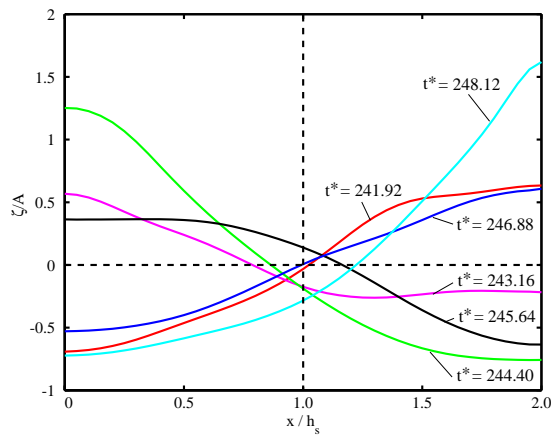


Fig. 11. Wave profiles in stable region for $\omega_1/\omega_F = 0.9$ and $\kappa = 0.017$. $\varepsilon = 0.288$, grid size of 40×80 .

exhibit dispersion effects at the nodes, $x/h_s = 0.25, 0.75, 1.25$ and 1.75 , in a similar fashion to that observed for single standing waves. This finding is also evident in the results of Chern et al. (1999). Fig. 9 shows the physical mesh of the free sloshing motion for the maximum nonoverturning double standing waves ($\varepsilon = 0.38$) when the free surface has a maximum (peak) and minimum (trough) at the tank centre.

5. Sloshing motions in a 2-D vertically excited tank

The second set of tests is concerned with forced sloshing of liquid in a rectangular tank subjected to vertical base excitation, as might occur in an idealized earthquake. In the following, the free surface motions are examined for increasing wave steepness, inside and outside regions of parametric resonance (instability regions). It should be noted that Faraday waves occurring in a vertically base-excited tank are a classical example of a parametrically excited system. A general property of such a system is instability of the equilibrium state when the forcing frequency is twice the natural frequency of the system (Ibrahim et al., 2001). This instability is often referred to as parametric resonance. As far as the equilibrium state is the solution, no motion can be generated by this excitation other than when certain initial perturbations of the equilibrium state exist. If there is an unstable mode amongst the perturbations it will grow exponentially. This distinguishes parametric resonance from classical resonance due to forced motion of an oscillating system. Classical resonance occurs when the forcing frequency equals the natural frequency of the system, resulting in the amplitude of the solution growing linearly.

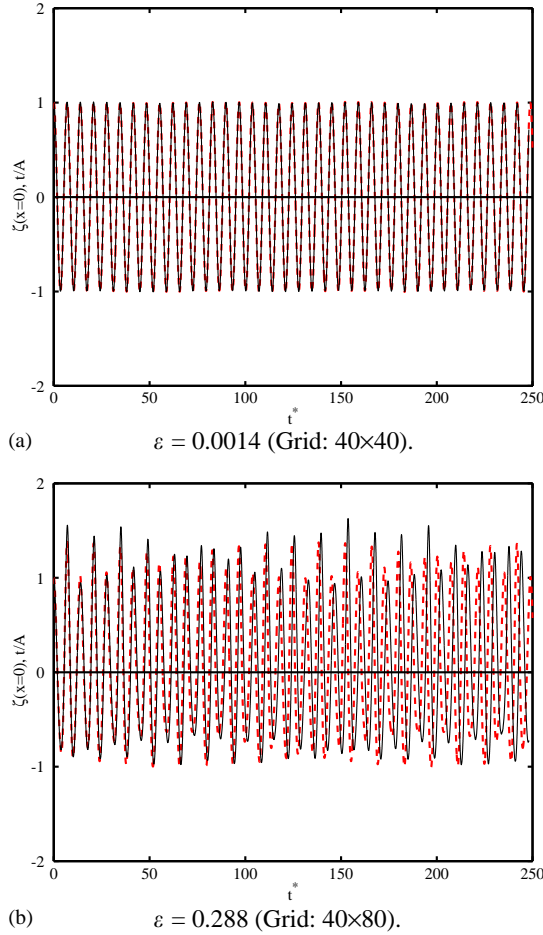


Fig. 12. Free-surface elevation in stable region at left wall for $\omega_1/\omega_F = 0.9$, and $\kappa = 0.017$. (a) $\varepsilon = 0.0014$ (Grid: 40×40). (b) $\varepsilon = 0.288$ (Grid: 40×80). —, Numerical prediction; - -, second-order solution.

We consider a 2-D tank excited by a vertical force at the base. The coordinate system is fixed at left wall of the tank, and moves with the tank. The dynamical free-surface boundary condition can be re-written as follows:

$$\frac{\partial \phi}{\partial t} = -\frac{1}{2}(\nabla \phi \cdot \nabla \phi) - \left(g + \frac{d^2 Z_F}{dt^2}\right) \zeta, \quad (17)$$

where Z_F is the forced vertical displacement of the tank. Using the σ -transformation at $\sigma = n_2$, Eq. (17) becomes

$$\frac{\partial \Phi}{\partial T} = \frac{(n_2 - n_1)}{h} \frac{\partial \zeta}{\partial T} \frac{\partial \Phi}{\partial \sigma} - (g - \omega_F^2 a \cos(\omega_F t)) \zeta - \frac{1}{2} \left[\frac{(m_2 - m_1)^2}{b^2} \left(\frac{\partial \Phi}{\partial X} - \frac{(n_2 - n_1)}{h} \frac{\partial \zeta}{\partial X} \frac{\partial \Phi}{\partial \sigma} \right)^2 + \frac{(n_2 - n_1)^2}{h^2} \left(\frac{\partial \Phi}{\partial \sigma} \right)^2 \right], \quad (18)$$

where the tank is assumed periodically excited with the following vertical base acceleration:

$$\frac{d^2 Z_F}{dt^2} = -\omega_F^2 a \cos(\omega_F t) \quad (19)$$

and where a is the forcing amplitude, t is the time and ω_F is the angular frequency of forced motion. The initial conditions are similar to the sloshing motion simulation in a fixed tank

$$\zeta(x, n)|_{t=0} = A \cos(k_n x) \quad (20)$$

and

$$\phi(x, z)|_{t=0} = 0. \quad (21)$$

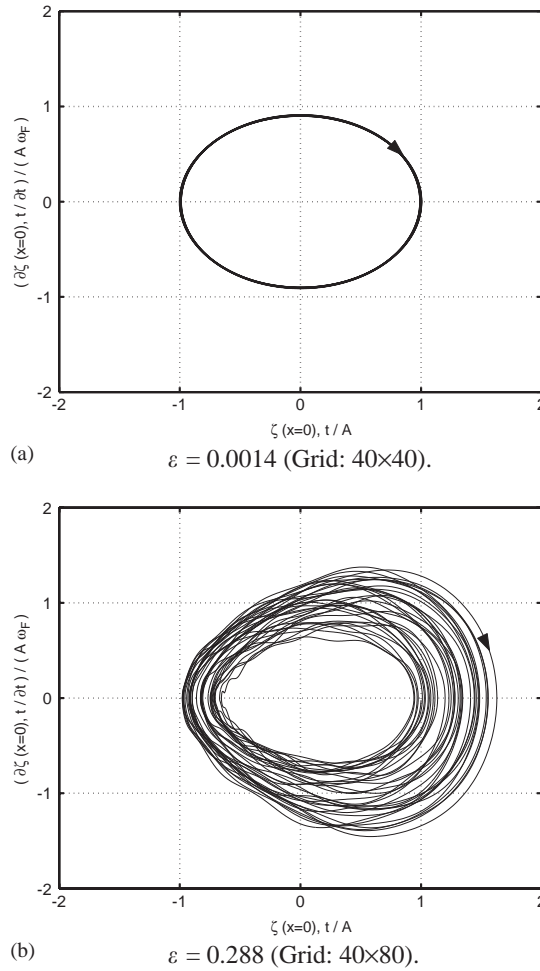


Fig. 13. Phase-plane plot in stable region at the left wall for $\omega_1/\omega_F = 0.9$, and $\kappa = 0.017$. (a) $\varepsilon = 0.0014$ (Grid: 40×40). (b) $\varepsilon = 0.288$ (Grid: 40×80).

Standing waves in vertically excited tanks, as originally explored in Faraday’s experiment, have been the subject of much attention (e.g. the review paper by [Miles and Henderson \(1990\)](#) and the recent work by [Jiang et al. \(1996\)](#), [Jiang et al. \(1998\)](#)). The linear solution for the motion of fluids in a vertically excited tank was first obtained by [Benjamin and Ursell \(1954\)](#). The second-order analytical solution for the free-surface elevation for the vertical base-excited tank satisfying the initial conditions for the n_{th} sloshing mode may be expressed:

$$\zeta(x, t) = A \left[\frac{\cos(k_n x)}{1 - \kappa \sin(\omega_F t)} T(\omega_F t) + \varepsilon \left(\frac{1}{2(1 - \kappa \sin(\omega_F t))} (1 + \cos(2k_n x)) T'(\omega_F t)^2 + \frac{-\Omega_n^2}{4(1 - \kappa \sin(\omega_F t))} \right. \right. \\ \left. \left. \times \left[1 + \frac{g^2 k^2}{\omega_n^4} + \left(1 - \frac{g^2 k^2}{\omega_n^4} \right) \cos(2k_n x) \right] T(\omega_F t)^2 + \frac{G'(\omega_F t)}{2(1 - \kappa \sin(\omega_F t))} + \frac{\cos(2k_n x) F'(\omega_F t)}{2(1 - \kappa \sin(\omega_F t))} \right) \right], \quad (22)$$

where the functions T , G and F satisfy the following ordinary differential equations:

$$T''(\tau) + \frac{\kappa \cos(\tau)}{1 - \kappa \sin(\tau)} T'(\tau) + \Omega_n^2 (1 - \kappa \sin(\tau)) T(\tau) = 0, \quad (23)$$

$$G''(\tau) + \frac{\kappa \cos(\tau)}{1 - \kappa \sin(\tau)} G'(\tau) = -\Omega_n^2 \left(\frac{k_n^2 g^2}{\omega_n^4} + 3 \right) T(\tau) T''(\tau) - \frac{\kappa \Omega_n^2 (\omega_n^4 + g^2 k_n^2) \cos(\tau)}{2\omega_n^4 (1 - \kappa \sin(\tau))} T(\tau)^2, \quad (24)$$

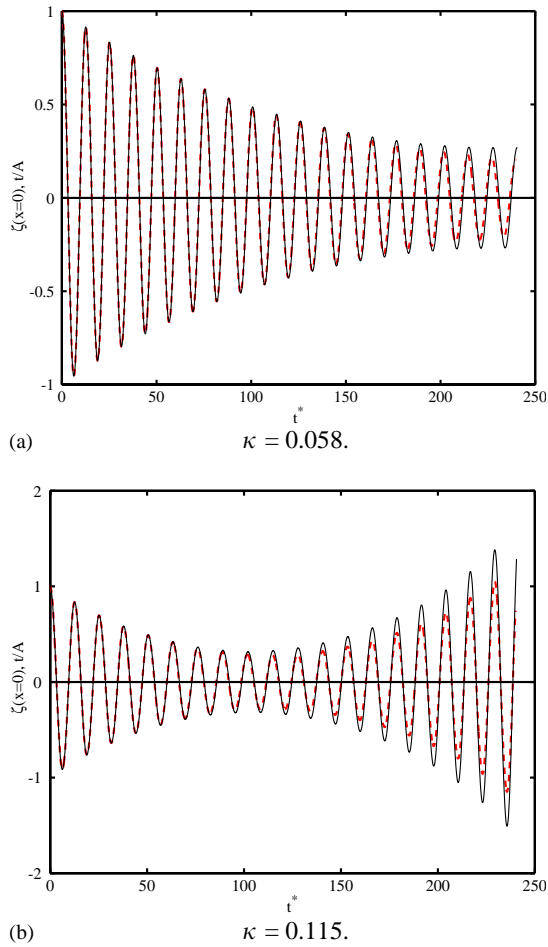


Fig. 14. Free-surface elevation in unstable region at the left wall for $\omega_1/\omega_F = 0.5$, and $\varepsilon = 0.0014$, and a grid size of 40×40 . (a) $\kappa = 0.058$. (b) $\kappa = 0.115$. —, Numerical prediction; - -, second-order solution.

and

$$F''(\tau) + \frac{\kappa \cos(\tau)}{1 - \kappa \sin(\tau)} F'(\tau) + \Omega_{2n}^2 (1 - \kappa \sin(\tau)) F(\tau) = 3\Omega_n^2 \left(\frac{k_n^2 g^2}{\omega_n^4} - 1 \right) T(\tau) T''(\tau) - \frac{\kappa \Omega_n^2 (\omega_n^4 - g^2 k_n^2) \cos(\tau)}{2\omega_n^4 (1 - \kappa \sin(\tau))} T(\tau)^2 \quad (25)$$

with initial conditions:

$$T(0) = G(0) = F(0) = 0, \quad T'(0) = G'(0) = F'(0) = 1$$

and

$$k_n = \frac{n\pi}{b}, \quad \omega_n = \sqrt{gk_n \tanh(k_n h_s)},$$

$$\Omega_n = \frac{\omega_n}{\omega_F}, \quad \Omega_{2n} = \frac{\omega_{2n}}{\omega_F}, \quad \kappa = \frac{a\omega_F^2}{g}, \quad \varepsilon = \frac{A\omega_n^2}{g}.$$

Note that the parameter κ is a measure of the importance of forcing motion and ε is a measure of nonlinearity.

Benjamin and Ursell (1954) also investigated the stability of this motion. They showed, that the solutions for the free-surface elevation can be expressed using Mathieu functions, $f(t)$, which satisfy the equation

$$\frac{\partial f}{\partial t} + (p - 2q \cos(2t))f(t) = 0. \quad (26)$$

The equation exhibits stable or unstable behaviour depending on the values of the parameters, p and q .

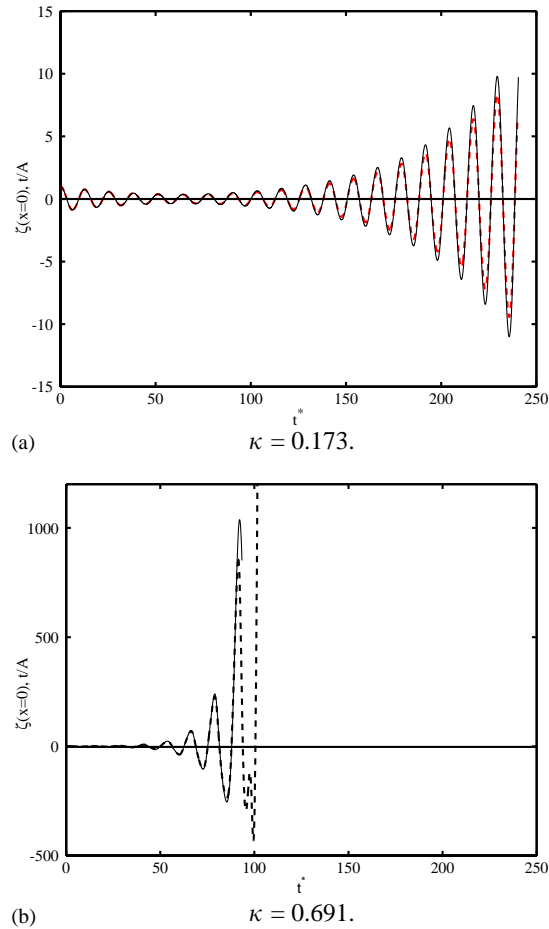


Fig. 15. Free-surface elevation in unstable region at the left wall for $\omega_1/\omega_F = 0.5$, and $\varepsilon = 0.0014$, and a grid size of 40×40 . (a) $\kappa = 0.173$. (b) $\kappa = 0.691$. —, Numerical prediction; - - -, second-order solution.

Eq. (23) for a function $T(\tau)$ can be reduced to Eq. (26) if we take $T(\tau) = f'(\tau/2 - \pi/4)$ and express the parameters as $\kappa = 2q/p$ and $\Omega_n^2 = p/4$. The corresponding stability map of Eq. (23) is represented in Fig. 10.

Further it should be noted that it is possible to obtain a first-order stable solution and a second-order unstable solution simultaneously. This occurs when the parameters (Ω_n, κ) lie in stable regions and the parameters (Ω_{2n}, κ) are in unstable regions. Note that the equation for the function $F(\tau)$ has the same differential operator as Eq. (23), and it produces an unstable solution that grows exponentially in time. The whole asymptotic expansion in this case becomes quickly nonuniformly invalid and the present form of the asymptotic solution can no longer be applied.

The test cases considered herein are marked on the stability map in Fig. 10. The first tests are carried out in a stable zone, with frequency ratio $\Omega_{n=1} = 0.9$, and a small nondimensional forcing amplitude, $\kappa = 0.017$. Fig. 11 illustrates the wave profiles across the tank at different times during a typical sloshing period for $\varepsilon = 0.288$. This is a steep wave case and significant influence of nonlinearity is evident in the asymmetric wave profiles and from the dispersion effects at the tank centre. The associated time history for the free-surface elevation is shown in Fig. 12b. As the solution evolves in time, a discrepancy in phase-shift between the numerical model and the approximate solution is evident; the fully nonlinear model predicts waves of slightly longer period than the approximate solution. Differences in amplitudes, of both peaks and troughs, can also be observed. The behaviour of the free surface motion in the vertical excited tank is similar to the standing waves observed in the fixed tank for this very small value of κ . Furthermore, it should be noted that for small nonlinearities ($\varepsilon = 0.0014$), a grid size of 40×40 resulted in sufficient accuracy in comparison with the second-order approximation (Fig. 12a). However, the steeper wave case ($\varepsilon = 0.288$) required a finer grid resolution of 40×80 . It was again found to be more effective to ensure accuracy by increasing the mesh density in the vertical direction than by higher resolution horizontally. We define the nondimensionalized time $t^* = \omega_F t$, and the nondimensional time step $\Delta t^* = \omega_F \Delta t$. Herein, a nondimensional time step of 0.012 was used for the test case in

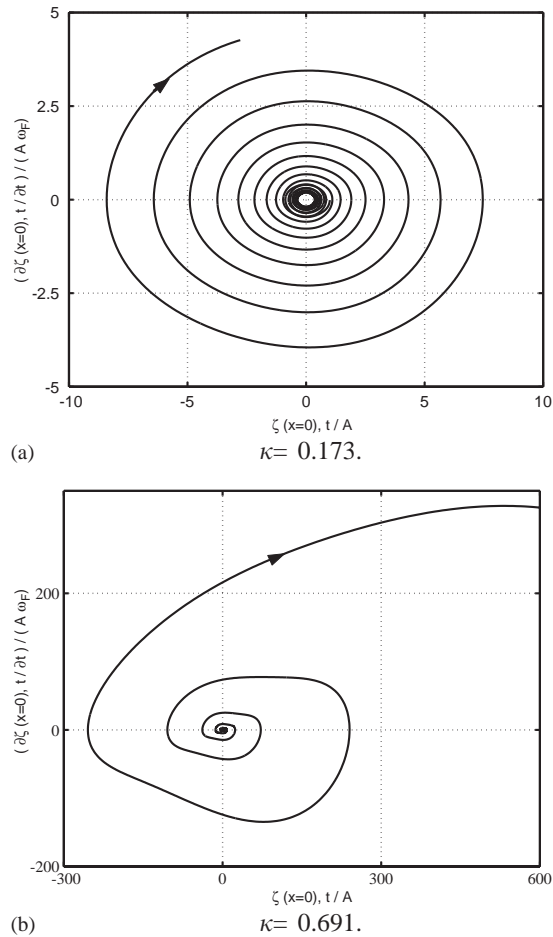


Fig. 16. Phase-plane plot in unstable region at the left wall for $\omega_1/\omega_F = 0.5$, and $\varepsilon = 0.0014$, and a grid size of 40×40 . (a) $\kappa = 0.173$. (b) $\kappa = 0.691$.

the stable region for both the small and steep wave cases. Fig. 13 presents the corresponding phase-plane plots for the small and steep wave cases. The small amplitude wave phase-plane plot (a) displays linear behaviour of the free surface that is exactly repeatable through the periodic closed orbit whereas the nonrepeatable nonclosed orbits of the large amplitude sloshing in (b) show that the free surface exhibits complicated behaviour typical of nonlinear systems.

Figs. 14 and 15 show the free-surface elevation time histories in the instability region for $\Omega_{n=1} = 0.5$. The forcing amplitude is varied from $\kappa = 0.058$ to 0.691 while the wave steepness parameter remains at a constant low value of $\varepsilon = 0.0014$. It can be seen that the free-surface elevation exhibits parametric resonance as expected in the region of instability. From $t^* = 0$ to approximately 100, i.e. during the no growth phase, the wave amplitudes predicted by the fully nonlinear model are found to be in close agreement with the second-order solution (26). When the amplitudes begin to grow at $t^* > 100$, discrepancies in amplitudes between the numerical model and the approximate analytical solution increase, as would be expected due to the enhanced nonlinearity of the free surface motions as t^* increases above 100. However, there is almost exact in-phase behaviour at all times. Fig. 16 shows phase-plane plots related to the free-surface time histories in Fig. 15. It can be observed that the free-surface exhibits standard linear behaviour for an unstable system.

Fig. 17 shows the free-surface time histories in the instability region for three values of ε while keeping the forcing amplitude small and constant ($\kappa = 0.057$). For small initial sloshing amplitudes, $\varepsilon = 0.0014$ and 0.014 , almost identical agreement for $t^* = 0-200$ is obtained between the fully nonlinear model and the second-order solution (Fig. 17a). After $t^* = 200$, some deviations in amplitude begin to occur, as anticipated. Nonlinear behaviour of the free-surface occurs when ε is increased to 0.144 (Fig. 17b). Excellent agreement with the approximate form is achieved for t^* from 0 to 100. Hereafter, deviations in amplitude and phase become evident. The associated wave profiles for

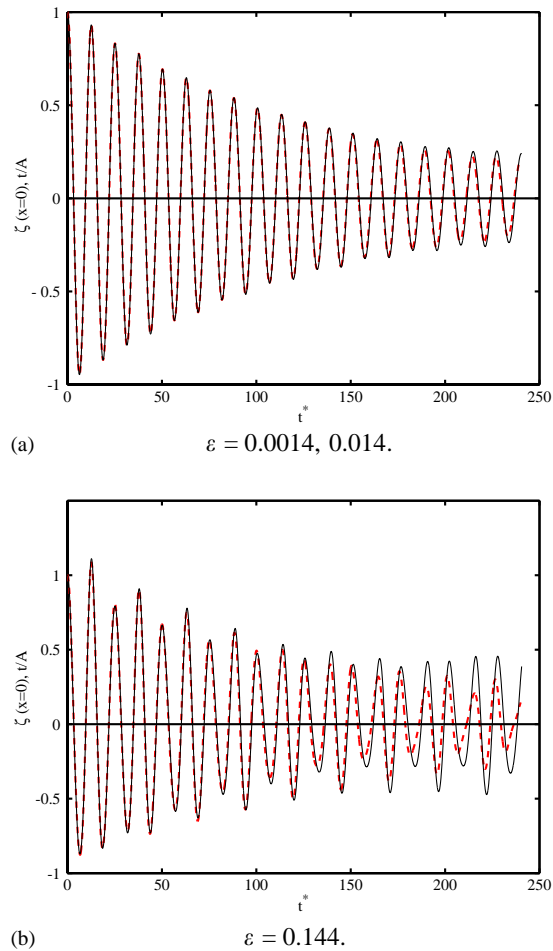


Fig. 17. Free-surface elevation in unstable region at the left wall for $\omega_1/\omega_F = 0.5$ and $\kappa = 0.057$, and a grid size of 40×80 . (a) $\varepsilon = 0.0014, 0.014$. (b) $\varepsilon = 0.144$. —, Numerical prediction; - -, second-order solution.

$\Omega_{n=1} = 0.5$ in the instability region are shown in Fig. 18 for small amplitude waves (a) and for large amplitude waves (b). The steep wave case reveals that asymmetric profiles and dispersion effects are evident at the tank centre, due to nonlinear effects.

The results presented herein are limited to a single liquid depth (for reasons of brevity). However, it is very important to note that the liquid depth has a profound influence on nonlinear free-surface effects. It has been established that there is a critical liquid depth that delineates two nonlinear regimes of the liquid free surface referred to as soft and hard spring characteristics. Gu and Sethna (1987), Gu et al. (1988) and Virnig et al. (1988) have examined the role of the liquid critical depth in rectangular tanks subjected to vertical sinusoidal excitation. Another important feature is that there is an excitation frequency range over which the free surface exhibits chaotic motion (Ibrahim et al., 2001). It is therefore intended in future to carry out a more exhaustive investigation of the complex free-surface behaviour under parametric excitation using the present model.

6. Conclusions

A fully nonlinear inviscid numerical wave tank has been developed based on potential flow theory with the mapped governing equations solved using a second-order finite difference scheme. Standing waves have been simulated in fixed and vertically moving 2-D rectangular tanks. Excellent agreement has been obtained between second-order potential theory solutions and the numerical model predictions for small amplitude wave cases. For steep sloshing, the numerical model captures the high-order nonlinear behaviour of the free-surface motions.

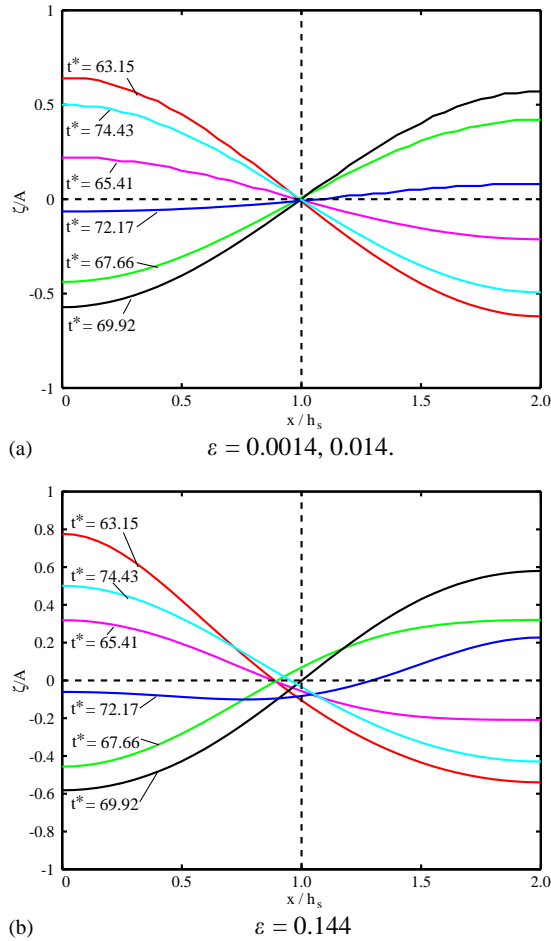


Fig. 18. Wave profiles in unstable region for $\omega_1/\omega_F = 0.5$ and $\kappa = 0.057$, and a grid size of 40×80 . (a) $\varepsilon = 0.0014, 0.014$. (b) $\varepsilon = 0.144$.

Sloshing effects in vertically excited tanks outside the unstable region display similar behaviour to free sloshing motions in a fixed tank when the forcing parameter, κ , is small. This confirms the periodic behaviour of the small amplitude solution. As κ increases, the fluid behaviour is no longer perfectly periodic, and irregular amplitudes occur, even for small amplitude waves. Nonlinear effects complicate the fluid behaviour further, making it almost unpredictable. However, in stable regions, the solution remains bounded at all times. Vertical motions produce drastic effects within the instability regions, where parametric resonance takes place. In these regions, tiny excitations can cause the growth of small initial perturbations, if the forcing acts on the tank for a sufficiently long time.

The present numerical model is simple, computationally cheap and accurate. For the cases considered in this paper, the σ -transformation removes the need for free-surface smoothing. The model provides a straightforward approach to simulating steep nonbreaking waves that may be readily extended to the prediction of 3-D wave motion.

Acknowledgements

The authors are grateful for stimulating discussions with members of the Ocean Engineering and Dynamics group at Oxford University, UK. In particular, we thank Professor Eatock Taylor for his advice. The second author also gratefully acknowledges support provided by the UK Engineering and Physical Sciences Research Council (EPSRC) under Grant GR/M56401.

References

- Abramson, H.N., 1966. The dynamics of liquids in moving containers. Report SP 106, NASA.
- Benjamin, T.B., Ursell, F., 1954. The stability of the plane free surface of a liquid in a vertical periodic motion. *Proceedings of the Royal Society (London), Series A* 225, 505–515.
- Bredmose, H., Brocchini, M., Peregrine, D.H., Thais, L., 2003. Experimental investigation and numerical modelling of steep forced water waves. *Journal of Fluid Mechanics*, in press.
- Chen, W., Haroun, M.A., Liu, F., 1996. Large amplitude liquid sloshing in seismically excited tanks. *Earthquake Engineering and Structural Dynamics* 25, 653–669.
- Chern, M.J., Borthwick, A.G.L., Eatock Taylor, R., 1999. A pseudospectral σ -transformation model of 2-D nonlinear waves. *Journal of Fluids & Structures* 13, 607–630.
- Faltinsen, O.M., 1978. A numerical non-linear method of sloshing in tanks with two dimensional flow. *Journal of Ship Research* 18 (4), 224–241.
- Faltinsen, O.M., Timokha, A., 2002. Asymptotic modal approximation of nonlinear resonant sloshing in a rectangular tank with small fluid depth. *Journal of Fluid Mechanics* 470, 319–357.
- Faraday, M., 1831. On a peculiar class of acoustical figures, and on certain forms assumed by groups of particles upon vibrating elastic surfaces. *Philosophical Transactions of the Royal Society of London* 121, 299–340.
- Ferrant, P., Le Touze, D., 2001. Simulation of sloshing waves in a 3D tank based on a pseudo-spectral method. In: *Proceedings of the 16th International Workshop on Water Waves and Floating Bodies*, Hiroshima, Japan.
- Frandsen, J.B., 2003. Sloshing motions in forced excited tanks. *Journal of Computational Physics*, in press.
- Greaves, D.M., Borthwick, A.G.L., Wu, G.X., Eatock Taylor, R., 1997. A moving boundary finite element method for fully non-linear wave simulations. *Journal of Ship Research* 41 (3), 181–194.
- Gu, X.M., Sethna, P.R., 1987. Resonance surface waves and chaotic phenomena. *Journal of Fluid Mechanics* 183, 543–565.
- Gu, X.M., Sethna, P.R., Narain, A., 1988. On three-dimensional nonlinear subharmonic resonance surface waves in a fluid: Part i—Theory. *Journal of Applied Mechanics* 55, 213–219.
- Ibrahim, R.A., Pilipchuk, V.N., Ikeda, T., 2001. Recent advances in liquid sloshing dynamics. *ASME Applied Mechanics Reviews* 54 (2), 133–199.
- Jiang, L., Perlin, M., Schultz, W.W., 1998. Period tripling and energy dissipation of breaking standing waves. *Journal of Fluid Mechanics* 369, 273–299.
- Jiang, L., Ting, C.-L., Perlin, M., Schultz, W.W., 1996. Moderate and steep Faraday waves: instabilities, modulation and temporal asymmetries. *Journal of Fluid Mechanics* 329, 275–307.
- Kareem, A., Kijewski, T., Tamura, Y., 1999. Mitigation of motions of tall buildings with specific examples of recent applications. *Journal of Wind and Structures* 2 (3), 201–251.
- Kocycit, M.B., Falconer, R.A., Lin, B., 2002. Three-dimensional numerical modelling of free surface flows with non-hydrostatic pressure. *International Journal for Numerical Methods in Fluids* 40, 1145–1162.
- Mellor, G.L., Blumberg, A.F., 1985. Modelling vertical and horizontal diffusivities with the sigma transform system. *Applied Ocean Research* 113, 1379–1383.
- Miles, J., Henderson, D., 1990. Parametrically forced surface waves. *Annual Review of Fluid Mechanics* 22, 143–165.
- Phillips, N.A., 1957. A coordinate system having some special advantages for numerical forecasting. *Journal of Meteorology* 14, 184–185.
- Tadjbakhsh, I., Keller, J.B., 1960. Standing surface waves of finite amplitude. *Journal of Fluid Mechanics* 8, 442–451.
- Telste, J.G., 1985. Calculation of fluid motion resulting from large amplitude forced heave motion of a two-dimensional cylinder in a free surface. In: *Proceedings of the Fourth International Conference on Numerical Ship Hydrodynamics*, Washington, USA, pp. 81–93.
- Tsai, C.-P., Jeng, D.-S., 1994. Numerical Fourier solutions of standing waves in finite water depth. *Applied Ocean Research* 16, 185–193.
- Turnbull, M.S., Borthwick, A.G.L., Eatock Taylor, R., 2003. Numerical wave tank based on a σ -transformed finite element inviscid flow solver. *International Journal for Numerical Methods in Fluids* 42, 641–663.
- Ushijima, S., 1998. Three-dimensional arbitrary Lagrangian–Eulerian numerical prediction method for non-linear free surface oscillation. *International Journal for Numerical Methods in Fluids* 26, 605–623.
- Vanden-Broeck, J.-M., Schwartz, L.W., 1981. Numerical calculation of standing waves in water of arbitrary uniform depth. *Physics of Fluids* 24 (5), 812–815.
- Virnig, J.C., Berman, A.S., Sethna, P.R., 1988. On three-dimensional nonlinear subharmonic resonance surface waves in a fluid: Part ii—Experiment. *Journal of Applied Mechanics* 55, 220–224.
- Wu, G.X., Eatock Taylor, R., Greaves, D.M., 2001. The effect of viscosity on the transient free-surface waves in a two-dimensional tank. *Journal of Engineering Mathematics* 40, 77–90.
- Wu, G.X., Ma, Q.A., Eatock Taylor, R., 1998. Numerical simulation of sloshing waves in a 3D tank based on a finite element method. *Applied Ocean Research* 20, 337–355.